Published in final edited form as:
Nanomedicine (Lond). 2010 July ; 5(5): 715–726. doi:10.2217/nnm.10.38.

Targeting of $\alpha_v\beta_3$-Integrins Expressed on Tumor Tissue and Neovasculature Using Fluorescent Small Molecules and Nanoparticles

Walter J Akers, DVM PhD,
Department of Radiology, Washington University School of Medicine

Zongren Zhang, PhD,
Department of Radiology, Washington University School of Medicine

Mikhail Berezin, PhD,
Department of Radiology, Washington University School of Medicine

Yunpeng Ye, PhD,
Department of Radiology, Washington University School of Medicine

Anthony Agee,
Department of Radiology, Washington University School of Medicine

Kevin Guo,
Department of Radiology, Washington University School of Medicine

Ralph W Fuhrhop,
Department of Medicine, Division of Cardiology, Washington University School of Medicine

Samuel A. Wickline,
Department of Medicine, Division of Cardiology, Washington University School of Medicine

Gregory M Lanza, MD PhD, and
Department of Medicine, Division of Cardiology, Washington University School of Medicine

Samuel Achilefu, PhD
Department of Radiology, Washington University School of Medicine

Abstract

Aims—Receptor-specific small molecules and nanoparticles are widely used in molecular imaging of tumors. Although some studies have described the relative strengths and weaknesses of the two approaches, reports of a direct comparison and analysis of the two strategies are lacking. Herein, we compared the tumor targeting characteristics of a small near-infrared (NIR) fluorescent compound (cypate –peptide conjugate) and a relatively large perfluorocarbon-based nanoparticles (250 nm diameter) for imaging $\alpha_v\beta_3$-integrin receptor expression in tumors.

Materials and Methods—NIR fluorescent small molecules and nanoparticles were administered to living mice bearing subcutaneous or intradermal syngeneic tumors and imaged with whole-body and high resolution optical imaging systems.

Results—The nanoparticles, designed for vascular constraint, remained within the tumor vasculature while the small integrin-avid ligand diffused into tissue to target integrin expression

Correspondence: Samuel Achilefu, PhD 4525 Scott Avenue, St. Louis, MO 63110 Fax: (314) 747-5191 Phone: (314) 747-0659 achilefus@wustl.edu.

on tumor and endothelial cells. Targeted small molecule and nanoparticle contrast agents preferentially accumulated in tumor tissue with tumor-to-muscle ratios of 8 and 7, respectively compared with 3 for non-targeted nanoparticles.

Conclusions—Fluorescent small molecular probes show greater overall early tumor contrast and rapid visualization of tumors, but the vascular-constrained nanoparticles are more selective for detecting cancer-induced angiogenesis. A combination of both imaging agents provides a strategy to image and quantify integrin expression in tumor tissue and tumor-induced neovascular system.

Keywords

perfluorocarbon; near-infrared; angiogenesis; fluorescence; $\alpha_v\beta_3$-integrin; cancer; optical imaging; peptide; emulsion

Introduction

Until recently, most imaging agents used in humans relied on small organic or inorganic molecules with typical hydrodynamic diameters less than a few nanometers. However, the emergence of nanotechnology has expanded the horizon of medical imaging to include nanoparticles as contrast agents. Both small molecules and nanoparticles have distinct advantages in molecular imaging. Nanoparticles offer a high surface to volume ratio that accommodates functionalization with multiple homing ligands for increased binding avidity or with contrast molecules for amplified imaging signal. [1] Moreover, nanoparticles can be engineered for vascular constraint, which eliminates confounding imaging signal from nontarget extravascular tissues. In contrast, small molecules targeted to diagnostic proteins can extravasate and bind a variety of cell types expressing the target biomolecules. In addition, rapid internalization of small molecules in cells can take advantage of receptor recycling pattern of a given target to improve overall tissue contrast relative to the surrounding.

Many studies have demonstrated the successful use of both small molecules and nanoparticles in receptor-mediated selective delivery of imaging agents and drugs to disease tissues. For example, proliferating tumors are known to generate new blood vessels, a process known as angiogenesis. Angiogenesis is an important microanatomical feature of tumor development characterized by the unique intraluminal expression of the $\alpha_v\beta_3$-integrin receptor on the surface of proliferating endothelial cells. [2,3] Therefore, contrast agents consisting of small molecules and nanoparticles targeted to $\alpha_v\beta_3$-integrin receptor have been used to image tumor neovasculature by nuclear, optical, ultrasound and magnetic resonance imaging methods. [4-6] For example, the ability of peptides possessing the arginine-glycine-aspartic acid (RGD) sequence to bind $\alpha_v\beta_3$-integrin receptors with high affinity allows their use to develop integrin-selective imaging agents.

Near-infrared (NIR) fluorescent dyes such as cypate are preferred for optical imaging in living animals because of the relative transparency of biological tissue to light in the 700 to 900 nm wavelength range [7]. The limited penetration of light in deep tissue confines its applications to shallow tissues and organs. However, this imaging method is exquisitely suitable for use in small animal models of human diseases, especially for preclinical studies. Previous studies show that conjugation of cypate to cyclo(RGDfK) peptide produced an integrin-avid molecular probe cypate-cRGDfK (Fig. 1) with selective tumor uptake in tumor-bearing mice.[8]

Similarly, a variety of $\alpha_v\beta_3$-integrin targeted nanoparticles have been developed.[1,5] We chose to examine $\alpha_v\beta_3$-integrin targeted perfluorocarbon-based nanoparticles (PFCNPs) with an average diameter of 250 nm as a flexible multifunctional platform for molecular imaging

and drug delivery.[9] In contrast to other commonly reported nanoparticle-based imaging agents, these nanoparticles are sufficiently large to remain within the vascular lumen, providing opportunity to evaluate only endothelial $\alpha_v\beta_3$ expression.[10] Additionally, a clear translational path is available since the particles are formulated with biocompatible materials.[9] Incorporation of homing ligands and imaging molecules into the encapsulating lipid surfactant monolayer afforded high sensitivity for noninvasive detection and characterization of cancer-induced angiogenesis in multiple animal studies. [11-17]

While both integrin-specific small molecules and nanoparticles have been used in molecular imaging of tumors, the relative strengths and weaknesses of the two approaches have never been directly examined. In this study, we prepared cypatecRGDfK peptide and NIR fluorescent $\alpha_v\beta_3$-integrin targeted PFC-NPs (cypate-PFC-tNPs) (Fig. 1) and evaluated these in mouse cancer models. The magnitude, as well as the spatial and temporal differences in tumor-related contrast generated by the highly penetrant fluorescent small molecule versus the vascular-constrained nanoparticle system were delineated to assess the clinical opportunities and challenges of each technology.

Materials and Methods

NIR fluorescent imaging agents

Cypate and cypate-cRGDfK (Fig. 1) were synthesized as previously reported. [7,8,18] A hydrophobic derivative of cypate, cypate-C18 (Fig. 1) was synthesized by conjugating cypate with 1-octadecylamine to increase hydrophobicity for inclusion in the hydrophobic core of the PFC-NPs. Cypate (30 mg, 1 eq.) was dissolved in 5 mL of DMF in a round bottom flask and 1-octadecylamine (2.1 eq.) HBTU (4 eq.) and DIEA (2 eq.) were added. After stirring at room temperature for 1 hour, DMF was evaporated under vacuum and the residue was re-dissolved in ethyl acetate, washed with saturated NaHCO3/water and brine, dried over MgSO4 and concentrated under vacuum. The product was purified by HPLC (water/acetonitrile w. 0.1% TFA) and lyophilized to give 7 mg of the desired compound as green powder. Yield: 12%, [M+]=1129. The fluorescent compound was used in nanoparticle formulation.

PFC-based nanoparticle formulation

NIR fluorescent cypate-PFC-NP (Fig. 1) were prepared by using similar methods described previously. [15,19] The emulsions comprised of 20% (v/v) perfluorooctylbromide (PFOB), 2.0% (w/v) of a surfactant co-mixture, and 1.7% (w/v) glycerin in distilled, deionized water. Targeted PFC-NPs (Fig. 1) were prepared by incorporating a peptidomimetic quinolone $\alpha_v\beta_3$ integrin antagonist targeting ligand developed by Bristol-Myers Squibb Medical Imaging. [16] The surfactant co-mixture of peptidomimetic nanoparticles included 98 mole% lecithin (Avanti Polar Lipids, Inc., Alabaster, AL, USA), 0.1 mole% of peptidomimetic quinolone conjugated to PEG_{2000}-phosphatidylethanolamine (Kereos, Inc, St. Louis, MO, USA), and 1.9 mole% phosphatidylethanolamine (Avanti Polar Lipids, Inc., Alabaster, AL, USA). Non-targeted nanoparticles excluded the quinolone ligand from the surfactant, which was replaced with equimolar phosphatidylethanolamine, a neutral phospholipid (Fig. 1). The surfactant components were combined with the PFOB, water, and glycerin, the pH was adjusted to 7.5, and the mixture was emulsified with an M110 microfluidizer (Microfluidics, Newton, MA, USA) at 20,000 psi for 4 minutes. For NIR fluorescent nanoparticles, the dye was substituted for lecithin on an equimolar basis at 0.1% and 0.3% for about 400 and 1200 molecules per nanoparticle, respectively. Nominal particle sizes and polydispersity (typically 250 nm with a polydispersity of 0.18) were measured with a dynamic light scattering technique (Brookhaven Instrument Corp., Holtsville, NY, USA).

Spectroscopy

Each sample (0.1 mL) was added to 0.9 mL of PBS in a cuvette and analyzed by absorption and fluorescence spectroscopy. The absorption spectra of the samples were recorded on a Beckman-Coulter DU-640 spectrophotometer (Fullerton CA). Fluorescence spectra were recorded on a Fluorolog III fluorometer (Horiba Jobin Yvon Inc., Edison NJ) with 720 nm excitation and 735-950 nm emission scan. Samples were measured in standard 1 cm quartz cells. Quantum yield was measured relative to ICG in DMSO. [20] All measurements were performed at room temperature. Fluorescence lifetime was measured using time correlated single photon counting (TCSPC) technique with NanoLed® 773 nm excitation source, impulse repetition rate 1 MHz at 90° to the detector (Hamamatsu Photonics, Shizuoka Japan). The detector was set to 820 nm with a 20 nm bandpass. The instrument response function (IRF) was obtained using Rayleigh scatter of Ludox - 40 (Sigma Aldrich, St. Louis MO) at a dispersion of 0.03% in MQ water in a quartz cuvette at 773 nm emission. DAS6 v6.1 decay analysis software (Horiba) was used for lifetime calculations. The fit was judged by χ^2 values and Durbin-Watson parameters and visual observations of fitted line, residuals and autocorrelation function. The lifetime was recorded on a 50 ns scale and a total of 8200 channels were used with time calibration 6.87×10^3 ns/channel.

Time-resolved emission spectroscopy (TRES) was conducted by using NanoLed® 773 nm excitation source and emission from 775 nm to 900 nm. Time gated traces were derived using TRES software package implemented in fluorescence decay analysis software DAS6 (Horiba).

Stability testing of the NIR dye in the lipid surfactant monolayer was performed by measuring fluorescent lifetime of the PFC nanoparticles in the presence of 0.1 % bovine serum albumin in PBS buffer (1 mL). The thermal stability of the nanoparticles was investigated by heating the cuvette to 90 °C using Peltier-type heating accessory.

Breast cancer models

All animal studies were performed in compliance with the Washington University School of Medicine Animal Studies Committee requirements for the humane care and use of laboratory animals in research. Luciferase-transfected 4T1 mouse mammary carcinoma cells (4T1*luc*) were cultured in Dulbecco's Modified Eagle Medium. Mice were anesthetized by intraperitoneal injection of ketamine and xylazine cocktail for injections and imaging procedures. All studies consisted of n=3 mice unless otherwise noted. For ear tumors, 1×10^4 cells in 0.01 mL were injected intradermally (ID) in each ear of female balb/c mice. For whole body imaging, 2×10^5 cells in 0.10 mL were injected subcutaneously (SQ) into the right shoulder of male NCR nude mice (Taconic Farms, Germantown, NY). Tumor location and size were visualized by bioluminescence imaging after intraperitoneal administration of 20 mg/kg D-luciferin potassium salt (Gold Biotechnology, St. Louis, MO). Bioluminescence signal was measured using Kodak IS4000MM (Carestream Health, Rochester, NY) imaging system (5 min, 8x8 binning). The camera dark noise was subtracted from the sum of the whole-ear ROIs to determine bioluminescence intensity using commercially available Molecular Imaging software (Carestream Health, New Haven, CT).

High resolution noninvasive tumor imaging

Three days following ID tumor cell implantation, mice (n=3) were anesthetized with isoflurane gas (2% v/v) and placed supine on the imaging platform of the NIR imaging system with MousePod accessory (Odyssey, Li-Cor Biosciences, Lincoln, NE). The imaging surface of mouse ears were coated with glycerin to improve resolution by eliminating surface-air interfaces. Mice were imaged individually at 0.02 mm per pixel in 800 nm channel.

After a pre-injection scan of the ears, either 0.10 mL of the nanoparticle solution (4×10^{13} particles/mL) or 0.02 mL (20 μM in 20% DMSO/water) cypate-cRGDfK was administered to the mouse by intravenous injection via lateral tail vein. Mouse ears were imaged at different time points: before, immediately after, 4 hours and 24 hours after injection. Injections and imaging were repeated on days 8 and 15 after tumor implantation. The fluorescence intensity within the blood vessels was compared with that of the nonvascular tissue to determine relative contrast.

ROIs were selected for the tumor region of the ear. Injected dose was estimated by measuring the fluorescence intensity from blood vessel ROIs in the post-injection image for each ear. ROIs were hand-drawn for tumors and mean signal intensity measured. The remaining pixels were selected as a second ROI and background intensity determined. Tumor-specific intensity was determined by subtracting background intensity from tumor intensity. These determined intensities were then normalized by injected dose as determined above.

Whole-body imaging and biodistribution

The biodistribution of imaging agents in male nude mice with SQ *4T1luc* tumors was assessed by whole-body planar fluorescence reflectance imaging. Images were acquired after intravenous administration of 100 μl of 20 μM cypate-cRGDfK (in 20% DMSO/water) or 150 μL of the nanoparticles solution. NIR fluorescence (755+/-35 nm excitation and 830 nm wide-angle emission filters, 60 second acquisition time), were acquired at 1, 4 and 24 hours after injection using the Kodak IS4000MM multimodal imaging system (Carestream Health, New Haven, CT). White light and digital X-ray images were acquired for anatomic reference. After the last imaging timepoint, mice were sacrificed and organ tissues were harvested and placed on a clear tray for fluorescence imaging. ROIs were selected using the automatic ROI selection function in the software by thresholding of the white light image and transfer of ROIs to the fluorescence image.

Statistical Analysis

ID tumor growth rates were compared by nonlinear regression to assess the biological effects of contrast agents on tumor growth. Growth rates were compared by evaluating differences in exponential growth rate (k) values between groups. For ID and subcutaneous tumor imaging, mean fluorescence intensities for ROIs were compared between groups using Student's t-test with $\alpha = 0.05$. Statistical analyses were performed using Graphpad Prism 5.0.

Results

NIR fluorescent dye and homing ligands

The NIR fluorescent dye, cypate was used as the fluorescent antenna for optical imaging. This dye was shown to have similar spectral properties and biodistribution profile in small animals as indocyanine green (ICG), a NIR fluorescent dye approved for human use. [21] Upon conjugation to a cyclic RGD peptide, the resultant molecular probe (Fig. 1) was shown to have high binding affinity to $\alpha_v\beta_3$–integrin receptor. [8] For nanoparticle formulation, we derivatized cypate with long alkyl chains to create a highly hydrophobic dye cypate-C18 (Fig. 1) suitable for encapsulation in the hydrophobic core of PFC-based nanoparticles. Stable nanoparticles were generated successfully (see below). We used the $\alpha_v\beta_3$–integrin antagonist [16] developed by Bristol-Myers Squibb Medical Imaging for this study. The quinolone nonpeptide ligand did not perturb the stability of the nanoparticles. This ligand was initially reported and characterized as the ^{111}In-DOTA conjugate RP748 and cyan 5.5 homologue TA145. [22] It had high specificity for $\alpha_v\beta_3$–integrin and a 15-fold

preference for the Mn^{2+} activated receptor (IC_{50} = 21 nM). [23] The IC_{50} values for $\alpha_v\beta_5$, $\alpha_5\beta_1$ and GP IIbIIIa proteins were determined to be >10 μM. [16]

Spectral analysis of fluorescent PFC-based nanoparticles

We determined the spectral properties of the cypate-C18, cypate-cRGDfK and the cypate-PFC-tNP. The absorption and emission properties of cypate-C18 and cypate-cRGDfK were essentially unchanged relative to non-conjugated cypate. Determination of the spectral properties of the PFC-based nanoparticles was more difficult because scattering dominated the absorption and emission spectra of the nanoparticles incorporating 0.1 and 0.3% NIR dye (Fig. 2). To minimize the effect of scattering, we subtracted the absorption spectral profile of control targeted PFC-NPs (non-fluorescent) from that of the cypate-PFC-NPs. The resulting spectra clearly show the presence of a near infrared dye in solution (Fig. 2), with strong absorption peaks detected at 680 nm and 797 nm demonstrating stable incorporation of the dye in the hydrophobic layer. Fluorescence peak at ~ 815 nm was obscurred by light scattering (not shown here), but became more apparent using TRES spectroscopy. The spectrum of the nanoparticle at 5 ns after excitation is shown in Fig. 2B. Stability of the fluorescence intensity after adding albumin to the emulsion suggests that the dye was well retained in the nanoparticle surfactant. The NIR cypate-PFC-tNPs demonstrated high thermal stability for up to 15 min at 90 °C without a change in the absorption and emission spectra. Additional treatment of the preheated and cooled nanoparticles with albumin revealed no shift in emission, further indicating the stable retention of the cypate dye in the nanoparticle surfactant.

The tabulated optical properties of cypate, cypate-C18, cypate-cRGDfK and cypate-PFC, including absorption maxima $\lambda_{abs,}$, emission maxima $\lambda_{em,}$ molar absorptivity ε, quantum yield Φ, and fluorescence lifetime τ are given in Table 1. The choice of solvents for this study was dictated by solubility and stability factors. Cypate and cypate-C18 form non-emissive aggregates in aqueous solutions, while cypate-cRGDfK is stable in 20% DMSO/water due to the large hydrophilic peptide. Cypate-PFC Liposomes were stable in water and unstable in less polar solvents.

High resolution in vivo imaging

The ID tumor growth rate varied, with bioluminescence detected as early as 3 days after implantation. Imaging agents had no significant effect on the growth of tumor xenografts as determined by bioluminescence measurements (P = 0.94). The nanoparticles showed strong fluorescence *in vitro* and *in vivo* above 800 nm with high signal-to-background ratio (SBR)=4.5 ±0.8 .

In vivo fluorescence from ear vasculature was high relative to surrounding tissues immediately after injection of the nanoparticles (Fig. 3A), with vascular contrast sustained for up to 24 hours. Fluorescence intensity in the blood vessels after administration of the small molecular probes was relatively short-lived, reflecting the rapid systemic clearance and extravasation into tissues. The relative plasma clearance and extravasation kinetics of the small molecule and nanoparticle contrast agents produced the differences in the observed vascular contrast. The PFC-based nanoparticles possessed a significantly longer circulation half-life as well as reduced rate of extravasation due to larger size and biocompatible surface components, promoting the longer time for blood vessel visibility (Fig. 3A). Metabolism of the agents, particularly degradation of the nanoparticles, could also have affected the in vivo distribution and imaging contrast.

Selectivity of tumor uptake was quantified by ROI analysis, comparing the measured fluorescence intensity for the tumor to that of the surrounding ear tissue. Tumor and normal

vasculature were detected by high resolution imaging of intradermal tumors in mouse ears (Fig. 3A) while whole-body biodistribution of the NIR fluorescent contrast agents was assessed by planar fluorescence reflectance imaging *in vivo* (Fig. 3B) and in *ex vivo* tissue sections (Fig. 3C). The relative fluorescence intensity in the tumor region was much greater ($p<0.05$) for the cypate-PFC-tNPs than for the small molecules with (Fig. 4) showing 20-40% greater accumulation in the intradermal tumor area relative to the cypate-cRGDfK. The pharmacokinetic profile of fluorescence after nanoparticles administration matches that of other stable nanoparticles [10,24,25], indicating little or no loss of fluorescent contrast agent from nanoparticles in circulation.

Angiogenesis was not detectable with the cypate-PFC-tNP at 3 days post-implantation of the tumor cells. However, tumor contrast was obvious at 7 days, suggesting that new proliferating blood vessels had sprouted and luminally expressed the $\alpha_v\beta_3$-integrin which the cypate-PFC-tNP bound. The NIR contrast persisted in the tumor tissues for more than 24 hours and still showed contrast 3 days after injection. Consistent with prior reports [12-14,17], nontargeted cypate-PFC-NP also were entrapped within the disarrayed tumor neovasculature but with much less signal intensity than the targeted cypate-PFC-tNP. The nonspecific uptake of imaging agents is a limitation at this time due to biological and size-dependent considerations. Continued optimization of targeted imaging agents and techniques will improve the target-to-nontarget contrast. This difference in contrast is about twice greater for the targeted than nontargeted nanoparticles at 7 days post-implant of tumor cells (Fig. 4). Thereafter, the differences between the two types of particles decreased. Although some smaller nanoparticles, typically less than 100 nm, can penetrate within tumors in mouse models through the enhanced permeation and retention (EPR) effect, larger nanoparticles such as the PFC-NPs (250nm) typically do not [16]. We have previously observed very low nonspecific uptake of non-targeted small molecule contrast agents [18], thus a similar agent was not included in this study.

It is reasonable to speculate that the hydrophobic NIR dye delivered in the surfactant of the PFC nanoparticles was transferred into the target cells and subsequently into the tumor via a mechanism we have referred to as contact facilitated drug delivery [26,27]. Lipid-encapsulated PFC nanoparticles can form hemifusion membrane complexes after binding to the target cell [28]. The constituents of the nanoparticle surfactant are transferred passively to the outer leaflet of the target cell membrane and then through an ATP-dependent mechanism, the phospholipid related entities can be translocated to the inner bilayer leaflet providing contiguous transport throughout the inner cell membranes without endosomal sequestration [14]. The *in vivo* effectiveness of this mechanism of drug delivery has been repeatedly demonstrated in preclinical models of cancer, cardiovascular disease, and arthritis [9,15,16,19,29]. These data reflect this mechanism and illustrate how hydrophobic drugs, modeled by the NIR cypate dye in this study, may be carried systemically to tumor neovascular sites via $\alpha_v\beta_3$–integrin targeted nanoparticles, delivered locally into the targeted endothelial cells along the growth front, and eventually dispersed further into the tumor parenchyma over time. Moreover, the significant enhancement in dye accumulation appreciated with integrin-specific versus the nontargeted nanoagents emphasized the benefit of active targeting of nanomedicines over simple passive accumulation.

The fluorescence contrast in the intradermal tumor area was higher for both types of nanoparticles, cypate-PFC-tNPs and cypate-PFC-NPs, than that of the small molecular probe at all times. This difference in contrast can be attributed to the higher permeability of the small molecules and greater distribution in the tumor and normal extravascular tissues relative to the nanoparticles. The small molecular probe attained peak tumor-to-normal contrast at 4 hours post-injection, with similar contrast observed at 24 hours. Unlike the

nanoparticles, fluorescence from the small molecular probe was barely detectable 3 days after injection.

Whole-body imaging and *ex-vivo* biodistribution of imaging agents

Whole-body imaging of mice showed the fluorescent small molecular probe cypate-cRGDfK and nanoparticles cypate-PFC-tNPs provided sufficient contrast for noninvasive tumor detection *in vivo* (Fig. 3B). The imaging agents distributed throughout the body and accumulated highly in the liver region. Fluorescence from the small molecular probe was also detected in the kidneys. Tumor contrast was high for all the imaging agents at 24 hours post-injection. *In vivo* tumor contrast was 1.32 +/- 0.13 for cypate-cRGDfK and 1.57 +/- 0.15 for targeted nanoparticles.

The relative biodistribution of the contrast agents was measured by *ex vivo* fluorescence imaging. The fluorescent nanoparticles showed high accumulation in the spleen and liver (Fig. 3C), while the small molecular probe concentrated in the liver and kidneys (not shown). Uptake in the spleen is expected for the relatively large nanoparticulates. [14,24] High tumor accumulation occurred for both cypate-cRGD and cypate-PFC-tNPs and with tumor-to-muscle ratios of 8.1 and 6.9, respectively compared with 3.0 for non-targed cypate-PFC-NPs (Figure 5). Other reports corroborate this finding for long-circulating biocompatible nanoparticles [13,14] and the potential effect of this undesirable uptake should be considered in the design and evaluation of targeted agents.

Discussion

Molecular imaging with optical contrast agents holds many advantages in preclinical imaging and it has made significant inroads to clinical applications.[30] Because of its high detection sensitivity, optical imaging is ideally suited for imaging molecular processes. For example, $\alpha_v\beta_3$–integrin receptor is highly expressed by proliferative cells such as white blood cells, immature endothelial cells and many types of cancer cells. [3,4] Therefore, small molecular contrast agents based on the $\alpha_v\beta_3$–integrin-avid RGD peptide motif have been extensively studied in preclinical models and some of these agents are under investigation for tumor detection in humans.[3] The conventional dogma for targeting $\alpha_v\beta_3$-integrin in tumor imaging with small molecular probes is to improve the tumor-to-normal tissue contrast. A major challenge in targeting tumor expressed $\alpha_v\beta_3$–integrin is its ubiquitous expression on cells of the immune system, cancer, and nascent endothelial cells. In such cases where the molecular target is expressed by a variety of tissue types, contrast agents constrained to the vasculature are better suited to differentiate luminal targets.[5,31]

In this study, we used two different tumor models, intradermal and subcutaneous, to explore the effectiveness of generating contrast by using small molecular probes and nanoparticles. The intradermal tumor model provided a thin and well-vascularized small tumor tissue for optical imaging of tumors in the early growth phase. The high vascularization as early as 3 days post-implantation is useful for gauging the tumor perfusion. In this model, the extent of angiogenesis relative to tumor size appears highest at 7 days post-implantation.

Our results demonstrate that vascular-constrained nanoparticles are effective in detecting tumor-induced angiogenesis, while small molecular probes can identify the tumor tissue by extravasating and binding to the target tumor. This difference in the distribution of targeted imaging agents is clearly demonstrated in the intradermal tumor model. Extravasation of the small molecular probe reduced the tumor contrast at early time points because of the high signal from surrounding normal tissues. On the contrary, the targeted nanoparticles provided higher contrast than the more diffusible small molecular probe. The high and prolonged

uptake of the nanoparticles in the small tumors is likely due to the high density of nascent blood vessels in this tumor model.

The small molecular probe and nanoparticles had different contrast effects on the subcutaneous tumor model. Tumors implanted subcutaneously are generally characterized by poorly vascularized interior, with angiogenesis occurring primarily in the periphery. [16] This feature reflects the lower imaging contrast in tumor generated by the nanoparticle contrast than that of the small molecular probe. Unlike nanoparticles, the small molecular probe is capable of diffusing rapidly into the entire tumor tissue, giving it the opportunity to detect and bind $\alpha_v\beta_3$-integrin receptor expressed in proliferating tumor cells in the tumor matrix. These additional molecular targets are not available to the nanoparticles. This, the targeted small molecular probe gave optimal contrast much earlier than the nanoparticles due to higher tissue permeability and faster blood and tissue clearance. The nanoparticles remained within the vasculature for prolonged period, which allows thorough interrogation of $\alpha_v\beta_3$-integrin receptor expression within the blood vessels. [10,24] However, the long circulation time of the nanoparticles has the disadvantage of higher background signal at early imaging time points after injection of the optical imaging agent, which is not apparent with less sensitive techniques such as MRI [12,13]. In certain situations, long circulating imaging agents could be an asset in molecular imaging of diseases. Some target receptors are known to internalize in cells after binding of their ligands and subsequently returned to the cell surface to bind more ligands. In this case, the availability of the imaging agent in circulating blood would allow the receptor to bind more agents, thereby amplifying the local imaging signal through receptor-mediated endocytosis. Additionally, long retention time of imaging agents in tumors could be advantageous. These situations may include clinical settings when a longer time is necessary between administration and non-invasive imaging and intraoperative image guidance for tumor resection or biopsy.

Conclusion

We demonstrated the complementary aspects of using small molecular probes and nanoparticles in molecular imaging of tumors. The imaging contrast generated by these agents depends on the tumor model used. The relatively larger tumor size and smaller, localized angiogenic vessels in the subcutaneous than the intradermal tumor model favor the use of small molecular probes for tumor imaging and diagnosis. The small molecule contrast agent diffuses easily from the tumor vasculature and can target $\alpha_v\beta_3$–integrin expressed by tumor cells and endothelial cells, providing higher overall tumor detection sensitivity. However, the imaging contrast by the vascular-constrained NIR fluorescent nanoparticles more reliably reflected the angiogenesis-related luminal expression of $\alpha_v\beta_3$, and thus aggressiveness of the tumors. On the contrary, the fluorescent nanoparticles provided higher imaging contrast than the small molecular probes when we used the intradermal tumor model. The thin and well-vascularized model with high vascular density relative to the tumor size provided more binding sites for the nanoparticles at early time points, but the rapid extravasation of the small molecular probe increased background fluorescence, favoring the use of nanoparticles in the intradermal tumor model than the small molecular probes. Taken together, both molecular imaging strategies are useful for reporting $\alpha_v\beta_3$–integrin expressed by tumor cells and tumor-induced endothelial cells.

Future Perspective

Numerous new imaging agents have been described in recent years and many more are under development for molecular imaging applications using disparate reporting strategies such as small molecules and nanoparticles. As the field of molecular imaging advances, there is a need to provide guidance regarding the use of these diverse imaging agents. Here, we demonstrated the utility of two molecular imaging agents that target the same cell-

surface receptor but report different information based on the relative differences of target accessibility. We envision the combination of these small molecular reporters and nanoparticles to access tumor aggressiveness and viability. In the case of $\alpha_v\beta_3$–integrin receptor, nanoparticles could first be used to delineate tumor-induced angiogenesis and small molecular probes would report the proliferative potential of the tumor tissue. In developing new molecular probes for tumor imaging, the choice of animal model could influence the outcome. It is important to use different animal models to assess the robustness of imaging agent in identifying and reporting the molecular target with high tumor-to-surrounding tissue contrast. Beyond imaging application, a combination of both delivery methods could provide a comprehensive strategy to treat tumor tissue and inhibit angiogenesis.

Executive Summary

- There is potential synergy between small molecular probes and fluorescent nanoparticles approaches in cancer imaging.
    - ○ Vascular constraint of nanoparticle contrast agents yields selectivity for imaging tumor-induced angiogenesis relative to highly diffusible small molecular probes.
    - ○ The diffusivity of small molecules are important to interrogate integrin expression on the tumor tissue directly.
    - ○ Both approaches, therefore, could serve synergistically to provide a comprehensive analysis of integrin expression in tumor tissue and the neovascular system.
- Intradermal tumor model with high density tumor-induced angiogenesis favors high contrast using fluorescent nanoparticles but subcutaneous tumor with peripheral blood vessels require rapid diffusion to the target tumor tissue, thereby favoring small molecular probes. The thin ear tissue allowed the resolution of small blood vessels from nonvascular tissues by contrast agent fluorescence.

Acknowledgments

This work was supported in part by NIH grants: 1U54CA136398, R01 CA109754 and CO-07121. The authors would like to thank Gail Sudlow for excellent technical assistance.

References

1. Debbage P, Jaschke W. Molecular imaging with nanoparticles: Giant roles for dwarf actors. Histochem Cell Biol 2008;130(5):845–875. [PubMed: 18825403]
2. Kobayashi H, Lin Pc. Nanotechnology for antiangiogenic cancer therapy. Nanomed 2006;1(1):17–22.
3. Meyer A, Auernheimer J, Modlinger A, Kessler H. Targeting rgd recognizing integrins: Drug development, biomaterial research, tumor imaging and targeting. Curr Pharm Des 2006;12(22): 2723–2747. [PubMed: 16918408]
4. Dijkgraaf I, Beer Aj, Wester Hj. Application of rgd-containing peptides as imaging probes for alphavbeta3 expression. Front Biosci 2009;14:887–899. [PubMed: 19273106]
5. Cai W, Chen X. Multimodality molecular imaging of tumor angiogenesis. J Nucl Med 2008;49(Suppl 2):113S–128S. [PubMed: 18523069]
6. Kaufmann, Ba; Lindner, Jr. Molecular imaging with targeted contrast ultrasound. Curr Opin Biotechnol 2007;18(1):11–16. [PubMed: 17241779]

7. Ye Y, Li Wp, Anderson Cj, Kao J, Nikiforovich Gv, Achilefu S. Synthesis and characterization of a macrocyclic near-infrared optical scaffold. J Am Chem Soc 2003;125(26):7766–7767. [PubMed: 12822971]
8. Ye Y, Bloch S, Xu B, Achilefu S. Design, synthesis, and evaluation of near infrared fluorescent multimeric rgd peptides for targeting tumors. J Med Chem 2006;49(7):2268–2275. [PubMed: 16570923]
9. Tran, Td; Caruthers, Sd; Hughes, M., et al. Clinical applications of perfluorocarbon nanoparticles for molecular imaging and targeted therapeutics. Int J Nanomedicine 2007;2(4):515–526. [PubMed: 18203420]
10. Neubauer, Am; Sim, H.; Winter, Pm, et al. Nanoparticle pharmacokinetic profiling in vivo using magnetic resonance imaging. Magn Reson Med 2008;60(6):1353–1361. [PubMed: 19025903]
11. Anderson, Sa; Rader, Rk; Westlin, Wf, et al. Magnetic resonance contrast enhancement of neovasculature with alpha(v)beta(3)-targeted nanoparticles. Magn Reson Med 2000;44(3):433–439. [PubMed: 10975896]
12. Winter, Pm; Caruthers, Sd; Kassner, A., et al. Molecular imaging of angiogenesis in nascent vx-2 rabbit tumors using a novel alpha(nu)beta3-targeted nanoparticle and 1.5 tesla magnetic resonance imaging. Cancer Res 2003;63(18):5838–5843. [PubMed: 14522907]
13. Schmieder, Ah; Winter, Pm; Caruthers, Sd, et al. Molecular mr imaging of melanoma angiogenesis with alphanubeta3-targeted paramagnetic nanoparticles. Magn Reson Med 2005;53(3):621–627. [PubMed: 15723405]
14. Hu G, Lijowski M, Zhang H, et al. Imaging of vx-2 rabbit tumors with alpha(nu)beta3-integrin-targeted 111in nanoparticles. Int J Cancer 2007;120(9):1951–1957. [PubMed: 17278104]
15. Winter, Pm; Schmieder, Ah; Caruthers, Sd, et al. Minute dosages of alpha(nu)beta3-targeted fumagillin nanoparticles impair vx-2 tumor angiogenesis and development in rabbits. Faseb J 2008;22(8):2758–2767. [PubMed: 18362202]
16. Schmieder, Ah; Caruthers, Sd; Zhang, H., et al. Three-dimensional mr mapping of angiogenesis with alpha5beta1(alpha nu beta3)-targeted theranostic nanoparticles in the mda-mb-435 xenograft mouse model. Faseb J 2008;22(12):4179–4189. [PubMed: 18697838]
17. Lijowski M, Caruthers S, Hu G, et al. High sensitivity: High-resolution spect-ct/mr molecular imaging of angiogenesis in the vx2 model. Invest Radiol 2009;44(1):15–22. [PubMed: 18836386]
18. Edwards, Wb; Akers, Wj; Ye, Y., et al. Multimodal imaging of integrin receptor-positive tumors by bioluminescence, fluorescence, gamma scintigraphy, and single-photon emission computed tomography using a cyclic rgd peptide labeled with a near-infrared fluorescent dye and a radionuclide. Mol Imaging 2009;8(2):101–110. [PubMed: 19397855]
19. Winter, Pm; Neubauer, Am; Caruthers, Sd, et al. Endothelial alpha(v)beta3 integrin-targeted fumagillin nanoparticles inhibit angiogenesis in atherosclerosis. Arterioscler Thromb Vasc Biol 2006;26(9):2103–2109. [PubMed: 16825592]
20. Lakowicz, Jr. Principles of fluorescence spectroscopy.. In: Lakowicz, JR., editor. Principles of Fluorescence Spectroscopy. Springer; Berlin: 2006. ISBN 0-387-31278-12006
21. Achilefu S, Dorshow Rb, Bugaj Je, Rajagopalan R. Novel receptor-targeted fluorescent contrast agents for in vivo tumor imaging. Invest Radiol 2000;35(8):479–485. [PubMed: 10946975]
22. Meoli, Df; Sadeghi, Mm; Krassilnikova, S., et al. Noninvasive imaging of myocardial angiogenesis following experimental myocardial infarction. J Clin Invest 2004;113(12):1684–1691. [PubMed: 15199403]
23. Sadeghi, Mm; Krassilnikova, S.; Zhang, J., et al. Detection of injury-induced vascular remodeling by targeting activated alphavbeta3 integrin in vivo. Circulation 2004;110(1):84–90. [PubMed: 15210600]
24. Longmire M, Choyke Pl, Kobayashi H. Clearance properties of nano-sized particles and molecules as imaging agents: Considerations and caveats. Nanomed 2008;3(5):703–717.
25. Almutairi A, Akers Wj, Berezin My, Achilefu S, Frechet Jm. Monitoring the biodegradation of dendritic near-infrared nanoprobes by in vivo fluorescence imaging. Mol Pharm 2008;5(6):1103–1110. [PubMed: 19434857]

26. Lanza, Gm; Yu, X.; Winter, Pm, et al. Targeted antiproliferative drug delivery to vascular smooth muscle cells with a magnetic resonance imaging nanoparticle contrast agent: Implications for rational therapy of restenosis. Circulation 2002;106:2842–2847. [PubMed: 12451012]

27. Crowder, Kc; Hughes, Ms; Marsh, Jn, et al. Sonic activation of molecularly-targeted nanoparticles accelerates transmembrane lipid delivery to cancer cells through contact-mediated mechanisms: Implications for enhanced local drug delivery. Ultrasound Med Biol 2005;31(12):1693–1700. [PubMed: 16344131]

28. Soman N, Lanza G, Heuser J, Schlesinger P, Wickline S. Synthesis and characterization of stable fluorocarbon nanostructures as drug delivery vehicles for cytolytic peptides. Nano Lett 2008;8:1131–1136. [PubMed: 18302330]

29. Chen Y, Zheng G, Zhang Zh, et al. Metabolism-enhanced tumor localization by fluorescence imaging: In vivo animal studies. Opt Lett 2003;28(21):2070–2072. [PubMed: 14587818]

30. Luker, Gd; Luker, Ke. Optical imaging: Current applications and future directions. J Nucl Med 2008;49(1):1–4. [PubMed: 18077528]

31. Mulder, Wj; Castermans, K.; Van Beijnum, Jr, et al. Molecular imaging of tumor angiogenesis using alphavbeta3-integrin targeted multimodal quantum dots. Angiogenesis 2009;12(1):17–24. [PubMed: 19067197]

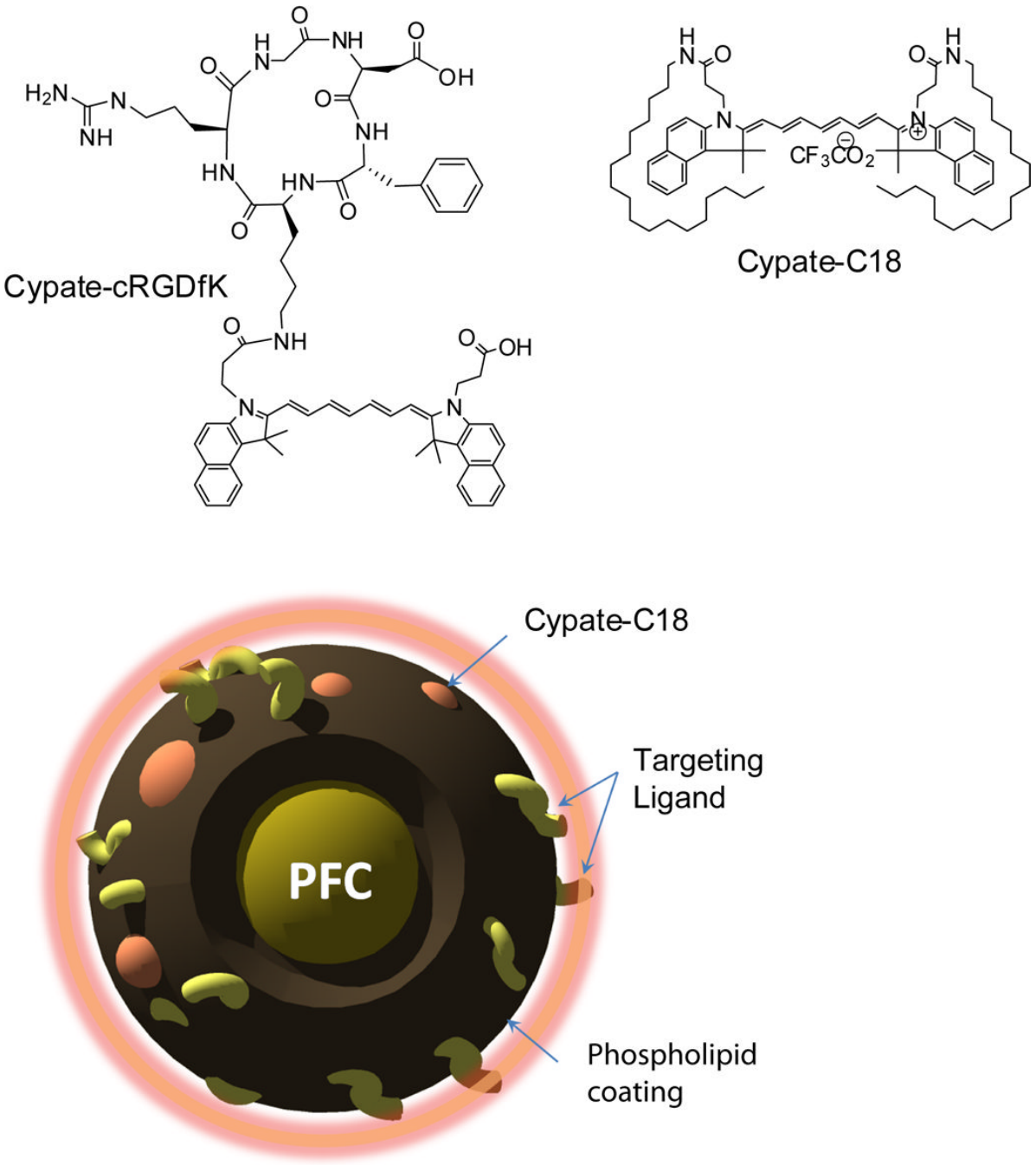

Figure 1.
Structures of small-molecule NIR fluorescent molecular probe, cypate-cRGDfK, dialkyl cypate derivative cypate-C18 and graphical depiction of targeted cypate PFC-tNP.

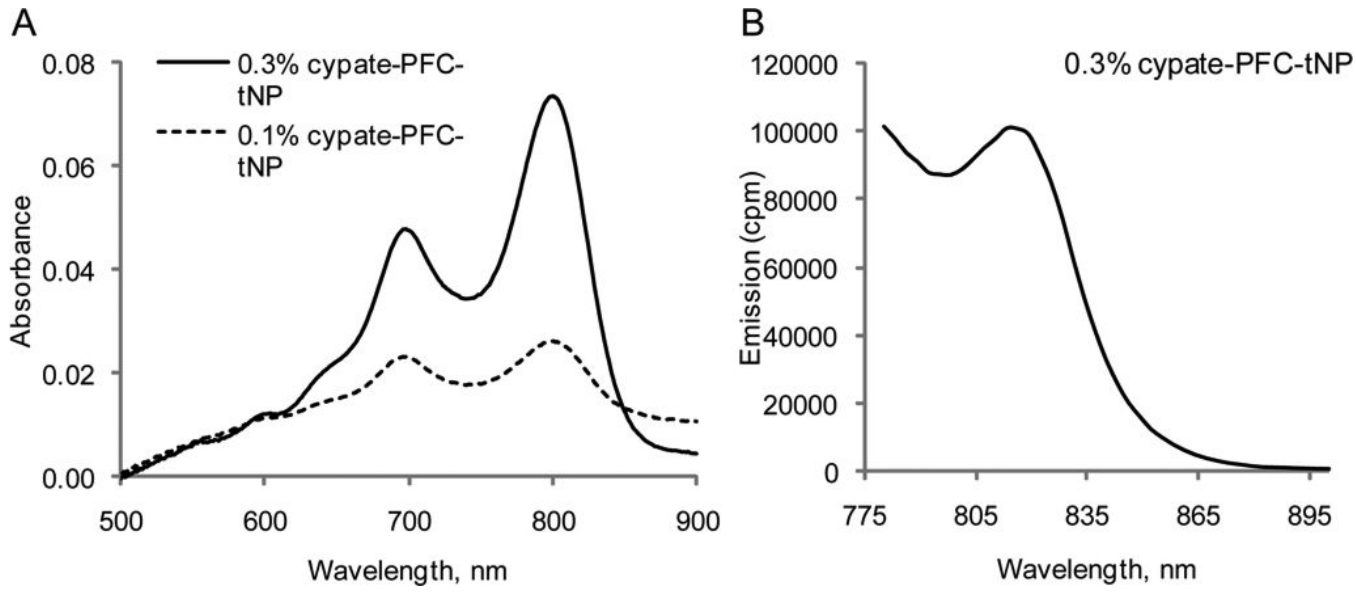

Figure 2.

(A) Absorption spectra of cypate-PFC-tNPs of two different loading in PBS buffer at room temperature. Absorption spectra were corrected for scattering by subtracting PFC-NPs. (B) Time-gated emission spectra of cypate-PFC-tNPs (5 ns after excitation) recorded using TRES (ex 773 nm)

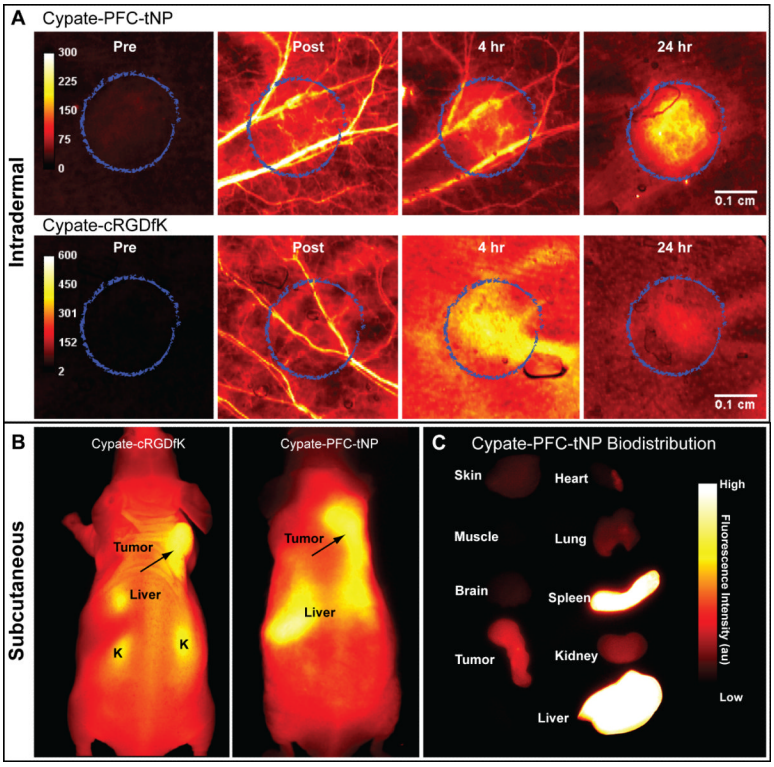

Figure 3.

(A) In vivo imaging of mouse ears with intradermal tumor region (circled) 9 days after implantation. Images were acquired by raster-scanning method at 21 μm per pixel, providing high resolution of tumor area. The cypate-PFC-tNPs long plasma residence time and delayed extravasation relative to cypate-cRGDfK vasculature was demonstrated by visibility of blood vessels for more than 4 hours after injection. (B) Whole-body NIR fluorescence images of mice bearing subcutaneous 4T1*luc* tumor 24 hours after injection of $\alpha_v\beta_3$-targeted cypate-cRGDfK (left) or targeted NIR fluorescent nanoparticles cypate-PFC-tNPs (right). (C) Fluorescence biodistribution imaging of *ex vivo* tissues 24 hours after fluorescent probe injection.

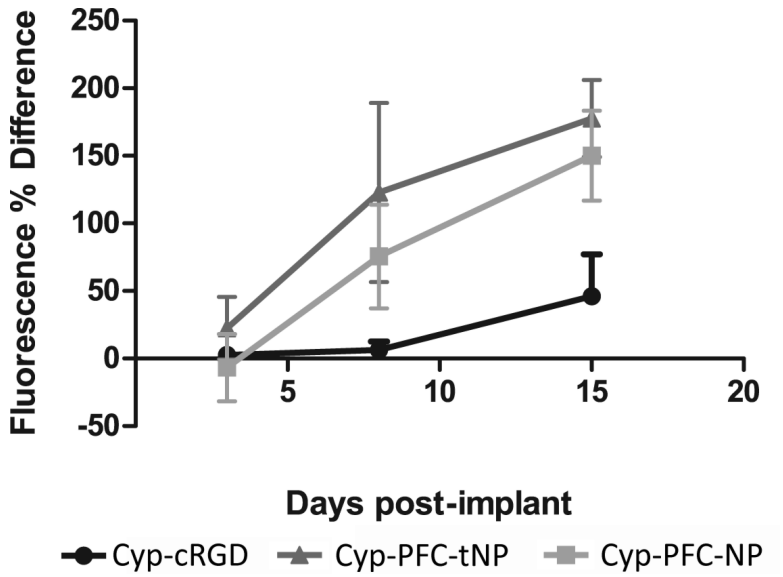

Figure 4.

Plot of NIR fluorescence intensity 24 hours after injection of non-targeted cypate-PFC-NPs or $\alpha_v\beta_3$-targeted targeted cypate-PFC-tNPs nanoparticles versus measured bioluminescence from tumors grown intradermally in mouse ears, 18 days post-implantation. Nonspecific accumulation due to the EPR effect is observed for the nanoparticles but it is significantly less than similar uptake observed for the targeted analogue. Uptake of the targeted nanoparticles is about twice that of the nontargeted analogue up to 7 days post-tumor cells implant. N=3, error bars indicate standard deviation.

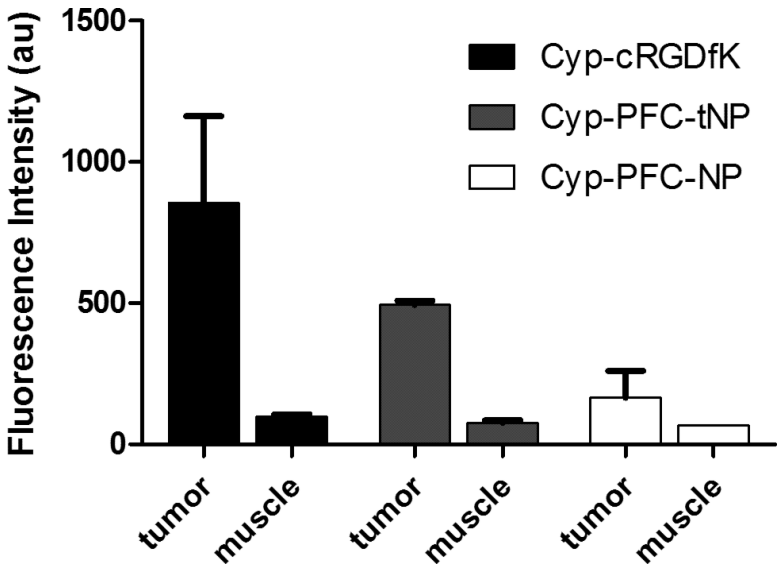

Figure 5.

Normalized fluorescence of *ex vivo* tumor and muscle tissues 24 hours after injection of NIR fluorescent imaging agents. $\alpha_v\beta_3$–integrin -targeted imaging agents showed significantly higher tumor specificity relative to non-targeted NIR fluorescent nanoparticles ($p<0.01$). Data for cypate-PFC-tNPs (2×10^{13} particles/ml, n=3 tumors) and cypate-cRGDfK (n=3) and for cypate-PFC-NPs (2×10^{13} particles/ml, n=2 tumors). Error bars indicate standard deviation.

Table 1

Spectroscopic properties of cypate based fluorescent probes

Entry	λ_{abs}, nm	λ_{em}, nm	$\varepsilon \times 10^{-3}$, M^{-1} cm^{-1}	Φ	τ, ns
cypate[a]	790	817	224	0.12	0.97
cypate-C18[a]	790	815	242	0.09	0.83
cypate-cRGDfK[b]	790	804	n/d	0.036	0.24
cypate-PFC-tNP[c]	797	813[d]	n/d[e]	n/d	n/d

[a] DMSO

[b] 20% DMSO/water

[c] water

[d] measured via TRES spectroscopy

[e] not determined because of small sample size.